Unfolding First-Principles Band Structures

Wei Ku (顧威),[1,2] Tom Berlijn,[1,2] and Chi-Cheng Lee (李啟正)[1]

[1]*Condensed Matter Physics and Materials Science Department, Brookhaven National Laboratory, Upton, New York 11973, USA*
[2]*Physics Department, State University of New York, Stony Brook, New York 11790, USA*
(Received 22 February 2010; published 24 May 2010)

A general method is presented to unfold band structures of first-principles supercell calculations with proper spectral weight, allowing easier visualization of the electronic structure and the degree of broken translational symmetry. The resulting unfolded band structures contain additional rich information from the Kohn-Sham orbitals, and absorb the structure factor that makes them ideal for a direct comparison with angle resolved photoemission spectroscopy experiments. With negligible computational expense via the use of Wannier functions, this simple method has great practical value in the studies of a wide range of materials containing impurities, vacancies, lattice distortions, or spontaneous long-range orders.

The electronic band structure is no doubt one of the most widely applied analysis tools in the first-principles electronic structure calculations of crystals, especially within the Kohn-Sham framework [1] of density functional theory [2]. It contains the basic ingredients to almost all the textbook descriptions of crystal properties (e.g., transport, optical and magnetic properties, and the semiclassical treatment [3]). Furthermore, the theoretical band structure, when formulated within the quasiparticle picture of the one-particle Green function, has a direct experimental connection with angle resolved photoemission spectroscopy (ARPES).

However, the usefulness of the band structure, as well as the agreement with ARPES spectra, diminishes rapidly when a large ''supercell'' is involved. The use of supercells is a common practice in modern first-principles studies when the original periodicity of the system is modified via the introduction of ''external'' influences from impurities or lattice distortions. They are also widely applied in the presence of spontaneous translational symmetry breaking, say, by a charge density wave, a spin density wave, or an orbital ordering. As illustrated in Fig. 1, when the period of the supercell grows longer, the corresponding first Brillouin zone of the supercell (SBZ) shrinks its size. In turn, bands in the first Brillouin zone of the normal cell (NBZ) get ''folded'' into the SBZ. For a very large supercell, the resulting SBZ can be tiny in size but contain a large number of ''horizontal'' looking bands that no longer resemble the original band structure or the experimental ARPES spectra, and cease to be informative besides giving a rough visualization of the density of states (DOS). The information is now hidden in the Kohn-Sham orbitals, instead of the dispersion of the bands.

In this Letter, by explicitly utilizing these Kohn-Sham orbitals, we present a method to unfold the band structure of the SBZ back to the larger NBZ with proper spectral weight. Making use of the corresponding Wannier functions, the method can be greatly simplified to negligible

computational cost. The resulting unfolded band structure incorporates explicitly the structure factor and thus facilitates significantly a direct comparison with ARPES experiments. Furthermore, the unfolded band structure illustrates very clearly the influence of the symmetry breaker (e.g., impurities, vacancies, dopants, lattice distortions) via direct comparison with the nominal normal-cell band structure. In the case of spontaneous symmetry breaking, it gives a direct visualization of the strength of each band's coupling to the order parameters. In light of the amazingly rich information, we expect countless applications of this simple method to a wide range of studies employing supercells, including systems with charge density wave, spin density wave, or orbital ordering, and in the studies of impurities and lattice distortions, to name a few.

Theoretically, the folding of the bands results from the introduction of additional coupling, $V_{kj,k'j'}$, between the originally uncoupled Kohn-Sham orbitals $|kj\rangle$ and $|k'j'\rangle$ in
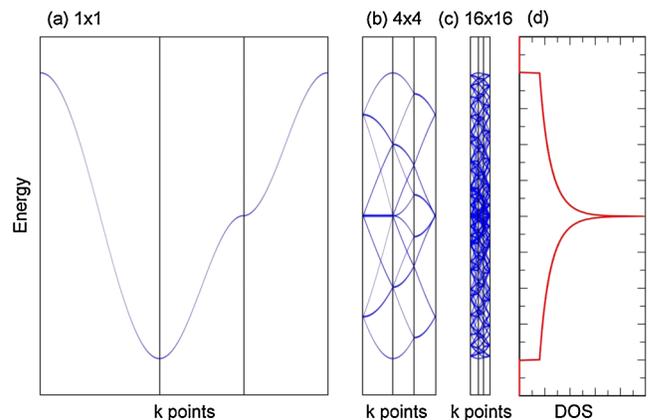
FIG. 1 (color online). Illustration of band folding in the supercell calculations: (a) band structure of a two-dimensional one-band first-neighbor tight-binding model, (b) the same obtained from a 4×4 supercell calculation, and (c) the same obtained from a 16×16 supercell calculation. Panel (d) shows the DOS.

the NBZ. (Here k and j denote the crystal momentum and the band index.) This coupling extends the period of Kohn-Sham orbitals to a longer one compatible with the size of the supercell. Equivalently, this coupling, no matter how small it is, mixes the original orbitals of different normal-cell crystal momentum k and forces us to label them with a supercell crystal momentum K as the new quantum number in the SBZ. [In the following, upper (lower) case symbols refer to variables corresponding to the super (normal) cell.] Our method is based on the simple idea that unless V is extremely strong, it is much more convenient and informative to represent the band structure or more precisely the spectral function $A = -\text{Im}G/\pi$ of the retarded one-particle Green function, G, not in the new eigenorbital $|KJ\rangle$ basis, but in the $|kj\rangle$ basis of the normal cell instead:

$$G^{-1}_{kj,k'j'}(\omega) = G^{-1}_{0kj,kj}(\omega)\delta_{k,k'}\delta_{j,j'} - V_{kj,k'j'}, \quad (1)$$

where G_0 represents a conceptual system with the period of the normal cell before V is applied. Clearly, G smoothly recovers the original period of G_0 as V approaches zero. Thus,

$$A_{kj,kj}(\omega) = \sum_{KJ}|\langle kj|KJ\rangle|^2 A_{KJ,KJ}(\omega) \quad (2)$$

should resemble the band structure of the normal cell with deviations in both the dispersion and in the spectral weight that reflect the effects of V. Note that while the coupling V introduces nondiagonal elements of $A_{kj,k'j'}(\omega)$, we focus only on the diagonal elements here for simplicity, without loss of generality. It is straightforward to show that in the case of $V = 0$, the weight of the bands that follow the bands of the normal cell is exactly one, and that of the rest of the folded bands vanishes. One thus recovers exactly the original band structure of the normal cell as expected. That is, the unfolded band structure is invariant against any arbitrary choice of supercell.

In addition, it is often desirable to also measure in each band the contribution of local orbitals with well-defined characters (e.g., p_x, d_{xz}, e_g, bonding, or antibonding). This can be achieved rigorously via the use of local Wannier orbitals $|rn\rangle$:

$$A_{kn,kn}(\omega) = \sum_{KJ}|\langle kn|KJ\rangle|^2 A_{KJ,KJ}(\omega), \quad (3)$$

where $|kn\rangle = \sum_r|rn\rangle\langle rn|kn\rangle = \sum_r|rn\rangle e^{ik\cdot r}/\sqrt{l}$ are the Fourier transform of the Wannier orbitals $|rn\rangle$ of orbital index n and associated with the lattice vector r. (Here l denotes the number of k points in the NBZ.) Given a consistent definition of the Wannier functions of the supercell calculation that maps $|RN\rangle$ of the supercell to $|R + r, n'\rangle$ of the normal cell, where $r = r(N)$ is a normal-cell lattice vector within the first supercell, and $n' = n'(N)$ is the corresponding normal-cell orbital index, the use of Wannier functions also reduces dramatically the

computational expense by turning the factor

$$
\begin{aligned}
\langle kn|KJ\rangle &= \sum_{RN}\langle kn|RN\rangle\langle RN|KN\rangle\langle KN|KJ\rangle \\
&= \sum_{RN}\langle kn|R + r(N), n'(N)\rangle\langle RN|KN\rangle\langle KN|KJ\rangle \\
&= \sqrt{1/Ll}\sum_{RN}e^{i(K-k)\cdot R}e^{-ik\cdot r(N)}\delta_{n,n'(N)}\langle KN|KJ\rangle \\
&= \sqrt{L/l}\sum_{N}e^{-ik\cdot r(N)}\delta_{n,n'(N)}\delta_{[k],K}\langle KN|KJ\rangle \quad (4)
\end{aligned}
$$

into merely a structure factor that is a sum of coefficients of the eigenorbital $|KJ\rangle$ of the supercell in the Wannier function basis, modulated by the proper phase that encapsulates the internal position in the supercell. Here $[k]$ denotes the k point folded into the SBZ from k. Since $A_{KJ,KJ}$ is just a delta function at the eigenvalue, $\delta(\omega - \epsilon_{KJ})$, this final expression in essence requires only a simple coding to plot all the eigenvalues of the supercell in the larger NBZ with proper weights.

Of course, the above definition only makes sense when the Wannier functions $|RN\rangle \leftrightarrow |rn\rangle$ and $|RN'\rangle \leftrightarrow |r'n\rangle$ (that are translational symmetric in the normal-cell unit: same n different r) are approximately identical. Therefore, the "gauge" [4] of constructing $|RN\rangle$ and $|RN'\rangle$ with the same n must be controlled accordingly. In the presence of a potential that breaks the translational symmetry of the normal cell, for example, coming from a change density wave, lattice distortions, impurities, etc., the commonly employed [5–7] maximally localized Wannier function [4] and other minimization-based methods [8,9] risk defining the gauge differently in the supercell in favor of better localization, and thus should be used with extreme caution. We found that a maximum projection method [10–12] with consistent projection between the normal cell and the supercell works well to satisfy this requirement. Equations (3) and (4) should in principle also be applicable in many existing codes employing atomic center local orbitals as basis [13–17], as long as the nonorthogonal nature of those bases is taken into account. Of course, these methods do not benefit from the energy resolution of the Wannier functions that allows unfolding only the bands within the physically relevant energy range.

The unfolded band structure also has an important direct connection to the ARPES measurement. For systems with enlarged unit cells due to weak symmetry breaking, the ARPES spectra typically show different band structures in different Brillouin zones of the supercell, distinctly different from the results of first-principles calculations, which have all the bands in the SBZ. In some cases, the observed ARPES spectra might even appear ignorant about the SBZ [18]. This significant mismatch is typically regarded as the effect of the "matrix element" and left unaddressed by both theorists and experimentalists, making a direct comparison very difficult. Within the "sudden approximation," the ARPES intensity is proportional to [19,20]

$$\sum_{KJ} |\mathbf{e} \cdot \langle f|\mathbf{p}|KJ\rangle|^2 A_{KJ,KJ}(\omega) \sim \sum_{KJkn} |\mathbf{e} \cdot \langle f|\mathbf{p}|kn\rangle|^2 |\langle kn|KJ\rangle|^2 A_{KJ,KJ}(\omega) = \sum_{kn} |\mathbf{e} \cdot \langle f|\mathbf{p}|kn\rangle|^2 A_{kn,kn}(\omega), \qquad (5)$$

where $\mathbf{e}$ denotes the polarization vector of light, and $|f\rangle$ the "final state" of the photoelectron. Clearly, except for the polarization dependent dipole matrix element, $|\mathbf{e} \cdot \langle f|\mathbf{p}|kn\rangle|^2$, the unfolded spectral function, $A_{kn,kn}(\omega)$, contains almost the full information of the experimental spectrum by absorbing the additional structure factor $\langle kn|KJ\rangle$, absent in the typical supercell solution, $A_{KJ,KJ}(\omega)$. Obviously, the inclusion of this additional matrix element would facilitate significantly the comparison between theory and the ARPES experiment.

As an example, let us consider the effect of Na impurities in Na-doped cobaltates, Na_xCoO_2 at $x = 1/3$. In typical first-principles studies [21,22], the impurity is incorporated via a supercell as demonstrated in Fig. 2(b) in comparison with the undoped normal cell shown in Fig. 2(a). Figures 2(c) and 2(d) show the corresponding band structures obtained with standard density-functional theory calculations. Since in this example the supercell is 3 times larger than the normal cell, the corresponding SBZ is 3 times smaller and contains 3 times more bands. Clearly, even for such a small supercell, the change of the size and

FIG. 2 (color online). Lattice structures of (a) Co_2O_4 (normal cell) and (b) $Na_2Co_6O_{12}$ (supercell), the corresponding band structure of (c) the normal cell and (d) supercell calculation, and (e) the unfolded band structure of the supercell. The inset illustrates the effects of weak translational symmetry breaking via spectral functions over the region $[-4.6 \text{ eV}, -4.2 \text{ eV}]$ and $[\frac{1}{5}M\Gamma, \frac{3}{5}M\Gamma]$.

orientation of the SBZ, and more importantly the large number of folded bands, make it practically impossible to cleanly compare with the band structure in the NBZ of the undoped parent compound. In fact, to many untrained eyes, these two band structures may appear entirely unrelated.

By contrast, the unfolded band structure shown in Fig. 2(e) demonstrates a strong resemblance to the band structure of the undoped compound. This allows a clear visualization of the effects of the (periodic) Na impurities on the original Co and O bands. Specifically, besides the introduction of additional Na-s bands, one observes shifts in band energies, gap openings, and the nearby "shadow bands," all of which reflects the influence of the Na impurity on these bands. What is really nice here is the cleanness of the unfolded band structure in general, owing to the weak intensity of the shadow bands. As expected, the influence of the Na impurity is only minor on most Co-d and O-p bands, while the Na-s bands themselves show sizable effects of broken translational symmetry. The size of the gap opening and the intensity of the shadow bands actually reflect directly the strength of each band's coupling to the broken translational symmetry of the normal cell (in this specific case, to the charge-density-wave (CDW) order parameter introduced by the periodic presence of Na atoms.) Of course, for a simulation of randomly positioned impurities, these CDW-related features are entirely artificial, and the unfolded band structure makes apparent the alarming limitation of the common practice of using small supercells in the study of impurities. On the other hand, in many other cases, for example the super modulation of the lattice, these features would actually correspond to a physical order parameter and provide valuable information.

As another example, let us consider a spontaneous orbital ordering in A-type antiferromagnetic $LaMnO_3$. Figures 3(c) and 3(d) show the similar comparison of band structures without and with the long-range staggered orbital order, corresponding to unit cells shown in Fig. 3(a) (normal cell) and Fig. 3(b) (supercell), respectively. Both results are obtained via the LSDA + U ($U = 8$ eV, $J_H = 0.88$ eV) approximation without lattice relaxation for simplicity, without loss of generality. By comparing the band structures with and without the orbital order on the equal footing, the detailed information of the spontaneous orbital order should be visualized explicitly.

Just like in the Na_xCoO_2 case, the straightforward results of the orbital ordered (OO) band structure [Fig. 3(d)] of the supercell calculation [23] can hardly be compared with the non-OO one [Fig. 3(c)]. By contrast, the unfolded band structure [Fig. 3(e)] of the OO case resembles strongly the non-OO case. In fact, one finds that only those bands of Mn-e_g character (red, blue, and green) show

FIG. 3 (color online).   Lattice structures of (a) normal cell and (b) doubled-size supercell of A-type antiferromagnetic ordered $LaMnO_3$, without and with the orbital ordering, respectively, the corresponding band structure of the normal cell (c) and the supercell (d), and the unfolded band structure of the supercell (e) indicating the orbital-ordering gap, Δ_{OO}. Red and blue bands denote the z^2 and $x^2 - y^2$ orbital characters of the spin-majority channel, and green bands give both e_g characters of the spin-minority channel.

strong coupling to the OO order parameter with large gap openings and intensive shadow bands, while the rest of the bands are basically uncoupled to the orbital order. In addition, from the significant energy gain corresponding to the large OO gap (Δ_{OO}) near the Fermi level of the red and blue bands, it is apparent that essentially the orbital order is driven only by the spin-majority e_g orbitals (red and blue). All these effects are of course entirely consistent with the existing "electronic interaction assisted Jahn-Teller picture" [24–26], in which the degenerate Mn-e_g orbitals split to gain energy and stabilize the system at low temperature. However, this unfolded band structure represents probably the best visualization of such physics in real materials with details of first-principles calculations.

In conclusion, a simple method for unfolding first-principles band structures of supercell calculations is presented. Proper spectral weights are obtained with negligible computational cost by making use of the Kohn-Sham orbitals with the help of carefully chosen Wannier functions. The inclusion of the structure factor in the resulting unfolded band structure makes it ideal for direct comparison with the ARPES measurement. The resulting unfolded band structures allow an easy visualization of each band's coupling to the order parameter of spontaneous broken translational symmetry, as well as their couplings to the external symmetry breakers such as the impurities and lattice distortions. Our method should prove valuable in the study of a wide range of problems requiring the use of supercells, including systems with impurities, vacancies, and lattice distortions, and broken symmetry phases of strongly correlated materials, to name a few.

[1] W. Kohn and L. J. Sham, Phys. Rev. **140**, A1133 (1965).
[2] P. Hohenberg and W. Kohn, Phys. Rev. **136**, B864 (1964).
[3] N. W. Ashcroft and N. D. Mermin, *Solid State Physics* (Holt, Rinehart, and Winston, New York, 1976).
[4] N. Marzari and D. Vanderbilt, Phys. Rev. B **56**, 12 847 (1997).
[5] K. S. Thygesen, L. B. Hansen, and K. W. Jacobsen, Phys. Rev. B **72**, 125119 (2005).
[6] X. Wang, J. R. Yates, I. Souza, and D. Vanderbilt, Phys. Rev. B **74**, 195118 (2006).
[7] A. Eiguren and C. Ambrosch-Draxl, Phys. Rev. B **78**, 045124 (2008).
[8] F. Gygi, J.-L. Fattebert, and E. Schwegler, Comput. Phys. Commun. **155**, 1 (2003).
[9] F. Giustino and A. Pasquarello, Phys. Rev. Lett. **96**, 216403 (2006).
[10] O. K. Andersen and T. Saha-Dasgupta, Phys. Rev. B **62**, R16219 (2000).
[11] W. Ku *et al.*, Phys. Rev. Lett. **89**, 167204 (2002).
[12] V. I. Anisimov *et al.*, Phys. Rev. B **71**, 125119 (2005).
[13] K. Koepernik and H. Eschrig, Phys. Rev. B **59**, 1743 (1999).
[14] V. Blum *et al.*, Comput. Phys. Commun. **180**, 2175 (2009).
[15] J. M. Soler *et al.*, J. Phys. Condens. Matter, **14**, 2745 (2002).
[16] M. J. Frisch *et al.*, GAUSSIAN 09, Revision A.1, Gaussian, Inc., Wallingford, CT, 2009.
[17] O. K. Andersen, Phys. Rev. B, **12**, 3060 (1975).
[18] S.-H. Lee *et al.*, arXiv:0912.3205.
[19] C. Caroli, D. Lederer-Rozenblatt, B. Roulet, and D. Saint-James, Phys. Rev. B **8**, 4552 (1973).
[20] M. Lindroos, S. Sahrakorpi, and A. Bansil, Phys. Rev. B **65**, 054514 (2002).
[21] D. J. Singh and D. Kasinathan, Phys. Rev. Lett. **97**, 016404 (2006).
[22] D. Pillay, M. D. Johannes, and I. I. Mazin, Phys. Rev. Lett. **101**, 246808 (2008).
[23] W. E. Pickett and D. J. Singh, Phys. Rev. B **53**, 1146 (1996).
[24] T. Hotta, A. L. Malvezzi, and E. Dagotto, Phys. Rev. B **62**, 9432 (2000).
[25] W.-G. Yin, D. Volja, and W. Ku, Phys. Rev. Lett. **96**, 116405 (2006).
[26] D. Volja, W.-G. Yin, and W. Ku, Europhys. Lett. **89**, 27 008 (2010).